Dynamical study of the Δ excitation in $N(e,e'\pi)$ reactions

T. Sato[1,2] and T.-S. H. Lee[2]
[1]*Department of Physics, Osaka University, Toyonaka, Osaka 560-0043, Japan*
[2]*Physics Division, Argonne National Laboratory, Argonne, Illinois 60439*
(Received 7 October 2000; published 27 March 2001)

The dynamical model developed by us [Phys. Rev. C **54**, 2660 (1996)] has been applied to investigate the pion electroproduction reactions on the nucleon. It is found that the model can describe to a very large extent the recent data of $p(e,e'\pi^0)$ reaction from Jefferson Laboratory and MIT-Bates. The extracted magnetic dipole ($M1$), electric dipole ($E2$), and Coulomb ($C2$) strengths of the $\gamma N\rightarrow\Delta$ transition are presented. It is found that the $C2/M1$ ratio drops significantly with Q^2 and reaches about -14% at $Q^2=4$ $(\mathrm{GeV}/c)^2$, while the $E2/M1$ ratio remains close to the value $\sim -3\%$ at the $Q^2=0$ photon point. The determined $M1$ transition form factor drops faster than the usual dipole form factor of the proton. We also find that the nonresonant interactions can dress the $\gamma N\rightarrow\Delta$ vertex to enhance strongly its strength at low Q^2, but much less at high Q^2. Predictions are presented for future experimental tests. Possible developments of the model are discussed.

DOI: 10.1103/PhysRevC.63.055201 PACS number(s): 13.75.Gx, 21.45.+v, 24.10.−i, 25.20.Lj

I. INTRODUCTION

One of the purposes of investigating the nucleon resonances (N^*) is to understand the nonperturbative dynamics of quantum chromodynamics (QCD). One possible approach to realize this is to compare the predictions of QCD-inspired models with the resonance parameters which can be extracted from the data of pion photoproduction and electroproduction reactions. In recent years, precise data including polarization observables have been obtained in the Δ region for pion photoproduction at LEGS [1] and Mainz [2], and for pion electroproduction at Thomas Jefferson National Accelerator Facility (JLab) [3,4], MIT-Bates [5], and NIKHEF [6]. These data now allow us to investigate more precisely the electromagnetic excitation of the Δ resonance.

In Ref. [7] we have developed a dynamical model (henceforth called the SL model) to extract the magnetic dipole ($M1$) and electric quadrapole ($E2$) strengths of the $\gamma N\rightarrow\Delta$ transition from the pion photoproduction data. The precise polarization data from LEGS and Mainz were essential in our analysis. In this paper, we report on the progress we have made in extending the SL model to investigate the pion electroproduction reactions in the Δ excitation region. We will make use of the recent data from JLab and MIT-Bates to explore the Q^2 dependence of the $\gamma N\rightarrow\Delta$ transition and make predictions for future experimental tests.

The dynamical content of the SL model has been given in detail in Ref. [7]. The essential feature of the model is to have a consistent description of both the πN scattering and the electromagnetic production of pions. This is achieved by using a unitary transformation method to derive an effective Hamiltonian defined in the subspace $\pi N\oplus\gamma N\oplus\Delta$ from the interaction Lagrangian for N,Δ,π,ρ,ω and photon fields. The resulting model has given a fairly successful description of the very extensive data for pion photoproduction. The extension of the SL model to investigate pion electroproduction is straightforward. The formulas needed for calculating the current matrix elements of pion electroproductions are identical to that given in Ref. [7] except that a form factor must be included at each photon vertex. Therefore no detailed presentation of our model will be repeated here. Similarly, we will not give detailed formulas for calculating the electroproduction cross sections since they are well documented [8–12].

The SL model is one of the dynamical models developed [7,13–21] in recent years. Compared with other approaches based on the tree diagrams of effective Lagrangian [22–25] or dispersion relations [26–28], the main objective of a dynamical approach is to separate the reaction mechanisms from the excitation of the internal structure of the hadrons involved. Within the SL model, this has been achieved by applying the well-established reaction theory within the Hamiltonian formulation (see, for example, Ref. [29]). In particular, the off-shell nonresonant contributions to the $\gamma N\rightarrow\Delta$ form factors can be calculated explicitly in a dynamical approach. Only when such nonresonant contributions are separated, the determined ''bare'' $\gamma N\rightarrow\Delta$ form factors can be compared with the predictions from hadron models. Within the SL model, this was explored in detail and provided a dynamical interpretation of the long-standing discrepancy between the empirically determined magnetic $M1$ strength of the $\gamma N\rightarrow\Delta$ transition and the predictions from constituent quark models. In this work, we further explore this problem utilizing the Q^2 dependence accessible to electroproduction reactions. Furthermore, the Coulomb (scalar) component $C2(S2)$ of the $\gamma N\rightarrow\Delta$ form factor will be determined.

In Sec. II, we briefly review the essential ingredients of the SL model and define various form factors which are needed to describe pion electroproduction reactions. With the Mainz data [2], we have slightly refined our model at the $Q^2=0$ photon point. This will be reported in Sec. III. The electroproduction results are presented and compared with the data in Sec. IV. In Sec. V, we give a summary and discuss possible future developments.

II. THE SL MODEL

Within the SL model, the pion photoproduction and electroproduction reactions are described in terms of photon and

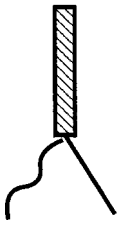

FIG. 1. Graphical representation of the $\gamma N \leftrightarrow \Delta$ interaction.

hadron degrees of freedom. The starting Hamiltonian is

$$H = H_0 + H_I, \tag{1}$$

with

$$H_I = \sum_{M,B,B'} \Gamma_{MB \leftrightarrow B'}, \tag{2}$$

where H_0 is the free Hamiltonian and $\Gamma_{MB \leftrightarrow B'}$ describes the absorption and emission of a meson (M) by a baryon (B). In the SL model, such a Hamiltonian is obtained from phenomenological Lagrangian for $N, \Delta, \pi, \rho, \omega$ and photon fields. In a more microscopic approach, this Hamiltonian can be defined in terms of a hadron model, as attempted, for example, in Ref. [30].

It is a nontrivial many body problem to calculate πN scattering and $\gamma N \to \pi N$ reaction amplitudes from the Hamiltonian (1). To obtain a manageable reaction model, a unitary transformation method [7,31] is used up to second order in H_I to derive an effective Hamiltonian. The essential idea of the employed unitary transformation method is to eliminate the unphysical vertex interactions $MB \to B'$ with $m_M + m_B < m_{B'}$ from the Hamiltonian and absorb their effects into $MB \to M'B'$ two-body interactions. In the SL model, the resulting effective Hamiltonian is defined in a subspace spanned by the πN, γN and Δ states and has the following form:

$$H_{eff} = H_0 + v_{\pi N} + v_{\gamma\pi} + \Gamma_{\pi N \leftrightarrow \Delta} + \Gamma_{\gamma N \leftrightarrow \Delta}, \tag{3}$$

where $v_{\pi N}$ is a nonresonant πN potential, and $v_{\gamma\pi}$ describes the nonresonant $\gamma N \leftrightarrow \pi N$ transition. The Δ excitation is described by the vertex interactions $\Gamma_{\gamma N \leftrightarrow \Delta}$ for the $\gamma N \leftrightarrow \Delta$ transition and $\Gamma_{\pi N \leftrightarrow \Delta}$ for the $\pi N \leftrightarrow \Delta$ transition. The vertex interaction $\Gamma_{\gamma N \leftrightarrow \Delta}$ is illustrated in Fig. 1. The nonresonant $v_{\gamma\pi}$ consists of the usual pseudovector Born terms, ρ and ω exchanges, and the crossed Δ term, as illustrated in Fig. 2 (the nonresonant term due to an intermediate anti-Δ state was found to be very weak and can be neglected). Most of the dynamical models have the above form of the Hamiltonian. However, the SL model has an important feature that the deduced effective Hamiltonian H_{eff} is energy independent and hermitian. Hence, the unitarity of the resulting reaction amplitudes is trivially satisfied. Furthermore, the nonresonant interactions $v_{\gamma\pi}$ and $v_{\pi N}$ are derived from the same H_I of Eq. (1), and hence the πN and γN reactions can be described consistently. Such a consistency is lost if $v_{\pi N}$ is either constructed purely phenomenologically as done in

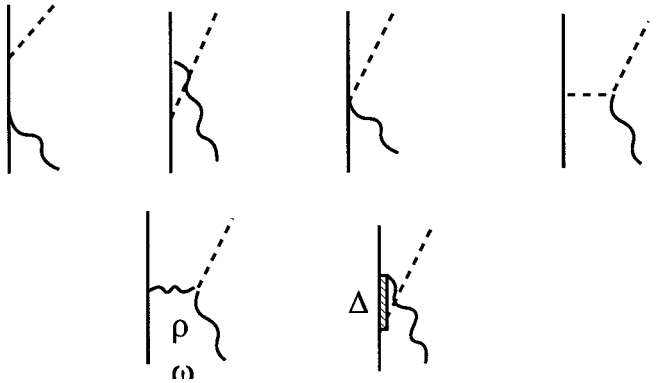

FIG. 2. Graphical representation of the nonresonant interaction of $v_{\gamma\pi}$ of Eq. (3). The waved, dashed, and solid lines denote the photon, pion, and nucleon, respectively.

Refs. [13–15] or taken from a different theoretical construction as done in Refs. [16,21]. This consistency is essential in interpreting the extracted $\gamma N \to \Delta$ form factors since the nonresonant interactions $v_{\pi N}$ and $v_{\gamma\pi}$ can dress the $\gamma N \to \Delta$ vertex. As discussed in Refs. [7,32], only the dressed $\gamma N \to \Delta$ transition can be identified with the data. The importance of the nonresonant effects on the $\gamma N \to \Delta$ transition is also stressed recently in Ref. [21].

From the effective Hamiltonian (3), it is straightforward to derive a set of coupled equations for πN and γN reactions. The resulting pion photoproduction amplitude can be written as

$$T_{\gamma\pi} = \langle \pi N | \epsilon \cdot J | \gamma N \rangle, \tag{4}$$

where J is the current operator and ϵ is the photon polarization vector. It can be decomposed into two parts

$$T_{\gamma\pi}(E) = t_{\gamma\pi}(E) + \frac{\bar{\Gamma}_{\Delta \to \pi N} \bar{\Gamma}_{\gamma N \to \Delta}}{E - m_\Delta - \Sigma_\Delta(E)}. \tag{5}$$

The nonresonant amplitude $t_{\gamma\pi}$ is calculated from $v_{\gamma\pi}$ by

$$t_{\gamma\pi}(E) = v_{\gamma\pi} + t_{\pi N}(E) G_{\pi N}(E) v_{\gamma\pi}, \tag{6}$$

where the πN free propagator is defined by

$$G_{\pi N}(E) = \frac{1}{E - E_N(k) - E_\pi(k) + i\epsilon}. \tag{7}$$

The amplitude $t_{\pi N}$ in Eq. (6) is calculated from the nonresonant πN interaction $v_{\pi N}$ by solving the following equation:

$$t_{\pi N}(E) = v_{\pi N} + v_{\pi N} G_{\pi N}(E) t_{\pi N}(E). \tag{8}$$

The dressed vertices in Eq. (5) are defined by

$$\bar{\Gamma}_{\gamma N \to \Delta} = \Gamma_{\gamma N \to \Delta} + \bar{\Gamma}_{\pi N \to \Delta} G_{\pi N}(E) v_{\gamma\pi}, \tag{9}$$

$$\bar{\Gamma}_{\Delta \to \pi N} = [1 + t_{\pi N}(E) G_{\pi N}(E)] \Gamma_{\Delta \to \pi N}. \tag{10}$$

In Eq. (9), we also have defined

$$\bar{\Gamma}_{\pi N\to\Delta}=\Gamma_{\pi N\to\Delta}[1+G_{\pi N}(E)t_{\pi N}(E)].$$

The Δ self-energy in Eq. (5) is then calculated from

$$\Sigma_\Delta(E)=\Gamma_{\pi N\to\Delta}G_{\pi N}(E)\bar{\Gamma}_{\Delta\to\pi N}. \tag{11}$$

As seen in the above equations, an important consequence of the dynamical model is that the influence of the nonresonant mechanisms on the resonance properties can be identified and calculated explicitly. The resonance position of the amplitude defined by Eq. (5) is shifted from the bare mass m_Δ by the self-energy $\Sigma_\Delta(E)$. The bare vertex $\Gamma_{\gamma N\to\Delta}$ is modified by the nonresonant interaction $v_{\gamma\pi}$ to give the dressed vertex $\bar{\Gamma}_{\gamma N\to\Delta}$, as defined by Eq. (9). In the SL model, it was found that the extracted $M1$ strength of the bare vertex $\Gamma_{\gamma N\to\Delta}$ is very close to the values predicted by the constituent quark models [33–35], while the empirical values given by the Particle Data Group (PDG) [36] can only be identified with the dressed vertex $\bar{\Gamma}_{\gamma N\to\Delta}$.

The above equations can be solved for arbitrary photon four-momentum $Q^2=-q^2>0$. For investigating the electroproduction reactions, we only need to define a form factor at each photon vertex in Figs. 1 and 2. For the nonresonant interactions (Fig. 2), we follow the previous work [10,11]. The usual electromagnetic nucleon form factors (given explicitly in Appendix A of Ref. [10]) are used in evaluating the direct and crossed nucleon terms. To make sure that the nonresonant term $v_{\gamma\pi}$ is gauge invariant, we set

$$F_A(q^2)=F_{\gamma\pi\pi}(q^2)=F_1^V(q^2), \tag{12}$$

where $F_A(q^2)$ is the form factor for the contact term, $F_{\gamma\pi\pi}(q^2)$ is the pion form factor for the pion-exchange term, and $F_1^V(q^2)$ is the nucleon isovector form factor (also given explicitly in Appendix A of Ref. [10]). The form factors for the vector meson-exchange terms are chosen to be

$$g_{V\pi\gamma}(q^2)=g_{V\pi\gamma}/(1-q^2/m_V), \tag{13}$$

where m_V is the vector meson mass and the coupling constants $g_{V\pi\gamma}$ for $V=\rho,\omega$ are deduced from the $V\to\gamma\pi$ decay widths and are given in Ref. [7]. The prescriptions (12) and (13) have been commonly used in most of the previous investigations such as that in Refs. [10,11]. Undoubtedly, this is an unsatisfactory aspect of this work. On the other hand, ''dynamically'' sound progress in solving the gauge invariance problem cannot be made unless a microscopic theory of hadron structure is implemented consistently into our model. This is beyond the scope of this work.

For the $\gamma N\to\Delta$ form factors, we follow the formulation developed by Jones and Scadron [37] and given explicitly in Refs. [10,15]. In the Δ rest frame where $m_\Delta=q_0+E_N(\vec{q})$, the resulting $\gamma N\to\Delta$ vertex function can be written in the following more transparent form:

$$\langle\Delta|\Gamma_{\gamma N\to\Delta}|q\rangle=-\frac{e}{(2\pi)^{3/2}}\sqrt{\frac{E_N(\vec{q})+m_N}{2E_N(\vec{q})}}\frac{1}{\sqrt{2\omega}}\frac{3(m_\Delta+m_N)}{4m_N(E_N(\vec{q})+m_N)}T_3\Big[iG_M(q^2)\vec{S}\times\vec{q}\cdot\vec{\epsilon}+G_E(q^2)(\vec{S}\cdot\vec{\epsilon}\vec{\sigma}\cdot\vec{q}+\vec{S}\cdot\vec{q}\vec{\sigma}\cdot\vec{\epsilon})$$
$$+\frac{G_C(q^2)}{m_\Delta}\vec{S}\cdot\vec{q}\vec{\sigma}\cdot\vec{q}\epsilon_0\Big], \tag{14}$$

where $e=\sqrt{4\pi/137}$, $q=(\omega,\vec{q})$ is the photon four-momentum, and $\epsilon=(\epsilon_0,\vec{\epsilon})$ is the photon polarization vector. The transition operators $\vec{S}$ and $\vec{T}$ are defined by the reduced matrix element $\langle\Delta||\vec{S}||N\rangle=\langle\Delta||\vec{T}||N\rangle=2$ in Edmonds' convention [38]. The parametrizations of the form factors $G_M(q^2)$, $G_E(q^2)$, and $G_C(q^2)$ will be specified in Sec. IV. By using Eq. (14) and the standard definitions [39,40] of multipole amplitudes, it is straightforward to evaluate the magnetic $M1$, electric $E2$, and Coulomb $C2$ amplitudes of the $\gamma N\to\Delta$ transition. We find [41] that

$$A_M(q^2)=[\Gamma_{\gamma N\to\Delta}]_{M1}=NG_M(q^2), \tag{15}$$

$$A_E(q^2)=[\Gamma_{\gamma N\to\Delta}]_{E2}=-NG_E(q^2), \tag{16}$$

$$A_C(q^2)=[\Gamma_{\gamma N\to\Delta}]_{C2}=N\frac{|\vec{q}|}{2m_\Delta}G_C(q^2), \tag{17}$$

with

$$N=\frac{e}{2m_N}\sqrt{\frac{m_\Delta|\vec{q}|}{m_N}}\frac{1}{[1-q^2/(m_N+m_\Delta)^2]^{1/2}}.$$

At $q^2=0$, the above relations agree with that given in Appendix A of Ref. [15].

At the $q^2=0$ photon point, we will also compare our results with the helicity amplitudes defined by PDG [36]. They are related to the multipole amplitudes defined above by

$$A_{3/2}=\frac{\sqrt{3}}{2}[A_E-A_M], \tag{18}$$

$$A_{1/2}=-\frac{1}{2}[3A_E+A_M]. \tag{19}$$

With the form factors defined in Eqs. (12)–(14), both the nonresonant term $v_{\gamma\pi}$ and the bare vertex $\Gamma_{\gamma N\to\Delta}$ are gauge invariant. However the full amplitude defined by Eq. (5) involves off-shell πN scattering, as defined by Eqs. (6)–(11), is not gauge invariant. There exists a simple prescription to

eliminate this problem phenomenologically. This amounts to defining the conserved currents for Eq. (4) as

$$J^\mu = J^\mu(SL) - \frac{q\cdot J(SL)}{n\cdot q} n^\mu, \tag{20}$$

where $J(SL)$ is calculated from our model defined above, and n is an arbitrary four vector. It is obvious that the currents J^μ defined by Eq. (20) satisfies the gauge invariance condition $q\cdot J=0$. If we use the standard choice of the photon momentum $q=(\omega,0,0,|\vec{q}|)$ and choose $n=(0,0,0,1)$, we then have

$$J_0 = J_0(SL),$$

$$J_x = J_x(SL),$$

$$J_y = J_y(SL), \tag{21}$$

and

$$J_z = J_z(SL) - \frac{\omega J_0(SL) - |\vec{q}| J_z(SL)}{-|\vec{q}|}\times 1 = \frac{\omega}{|\vec{q}|} J_0(SL). \tag{22}$$

The above equations mean that within our approach any $N(e,e'\pi)$ observable depending on the z component of the current is determined by Eq. (22) using the time component of the SL model, not by $J_z(SL)$. This is very similar to the prescription used in many nuclear calculations. We find that the data we have considered in this work can be described by the conserved currents J^μ defined by Eqs. (21) and (22). We have briefly investigated the model dependence due to the freedom in choosing n. We have found that the choice $n=(1,0,0,0)$, which leads to $\vec{J}=\vec{J}(SL)$ and $J_0=(|\vec{q}|/\omega)J_z(SL)$ gives very similar results at high Q^2. The differences at low Q^2 also appear to be not so large. All results presented in this paper are from using the choices (21) and (22). We emphasize that this choice is a phenomenological part of our model, simply because we have not implemented any substructure dynamics of hadrons into our formulation. In fact this is also the case for all existing approaches based on the prescription similar to the form of Eq. (20). For example $n=q$ is chosen in the recent work by Kamalov and Yang [21] using the dynamical model developed in Ref. [14]. There exist other prescriptions to fix the gauge invariance problem, such as those suggested in Refs. [44–46]. We have not explored those possibilities, since they are also not related microscopically to the substructure of the hadrons involved, and are as phenomenological as the prescription defined by Eqs. (21) and (22). We will return to this problem when our model is further developed, as discussed in Sec. V.

For our later discussions on the $\gamma N\to\Delta$ transition, we define some quantities in terms of more commonly used conventions. As discussed in detail in Ref. [7], if we replace the πN propagator $G_{\pi N}$ in Eqs. (5)–(11) by $G^K_{\pi N}(E)=P/[E-E_N(k)-E_\pi(k)]$ with P denoting the principal-value integration, the resulting dressed vertex $\bar{\Gamma}^K_{\gamma N\to\Delta}$ is real and can be directly compared with the bare vertex $\Gamma_{\gamma N\to\Delta}$. The usual $E2/M1$ ratio R_{EM} and $C2/M1$ ratio R_{SM} for the dressed $\gamma N\to\Delta$ vertex are then defined by

$$R_{EM} = \frac{[\bar{\Gamma}^K_{\gamma N\to\Delta}]_{E2}}{[\bar{\Gamma}^K_{\gamma N\to\Delta}]_{M1}}, \tag{23}$$

$$R_{SM} = \frac{[\bar{\Gamma}^K_{\gamma N\to\Delta}]_{C2}}{[\bar{\Gamma}^K_{\gamma N\to\Delta}]_{M1}}. \tag{24}$$

We note here that for the bare vertices defined by Eqs. (15)–(17), the $E2/M1$ and $C2/M1$ ratios can be simply related to the form factors: $[R_{EM}]^{bare}=-G_E(q^2)/G_M(q^2)$, $[R_{SM}]^{bare}=(|\vec{q}|/2m_\Delta)[G_C(q^2)/G_M(q^2)]$. The ratios (23) and (24) for the dressed vertices do not have such simple relations with the bare $\gamma N\to\Delta$ form factors. This is evident from Eqs. (9) and (10). Within our model, one can also show [7] that at the resonant energy where the invariant mass $W=1232$ MeV and the πN phase shift in the P_{33} channel goes through 90°, the multipole components of the dressed vertex $\bar{\Gamma}^K_{\gamma N\to\Delta}$ are related to the imaginary ($\mathrm{Im}\,M$) parts of the $\gamma N\to\pi N$ multipole amplitudes (as defined in Ref. [8]) in the πN P_{33} channel

$$\bar{A}_M = [\bar{\Gamma}^K_{\gamma N\to\Delta}]_{M1} = \sqrt{\frac{8\pi m_\Delta k\Gamma_\Delta}{3m_N q}}\times \mathrm{Im}(M^{3/2}_{1+}), \tag{25}$$

$$\bar{A}_E = [\bar{\Gamma}^K_{\gamma N\to\Delta}]_{E2} = \sqrt{\frac{8\pi m_\Delta k\Gamma_\Delta}{3m_N q}}\times \mathrm{Im}(E^{3/2}_{1+}), \tag{26}$$

$$\bar{A}_C = [\bar{\Gamma}^K_{\gamma N\to\Delta}]_{C2} = \sqrt{\frac{8\pi m_\Delta k\Gamma_\Delta}{3m_N q}}\times \mathrm{Im}(S^{3/2}_{1+}), \tag{27}$$

where Γ_Δ is the Δ width, k and q are respectively the momenta of the pion and photon in the rest frame of the Δ. Equations (25)–(27) agree with that given in Refs. [22,24]. From the above relations, we obtain a very useful relation that the $E2/M1$ ratio R_{EM} and $C2/M1$ ratio R_{SM} of the dressed $\gamma N\to\Delta$ transition at $W=1232$ MeV can be evaluated directly by using the $\gamma N\to\pi N$ multipole amplitudes

$$R_{EM} = \frac{\mathrm{Im}(E^{3/2}_{1+})}{\mathrm{Im}(M^{3/2}_{1+})}, \tag{28}$$

$$R_{SM} = \frac{\mathrm{Im}(S^{3/2}_{1+})}{\mathrm{Im}(M^{3/2}_{1+})}. \tag{29}$$

The formula for calculating the multipole amplitudes and various cross sections from the total amplitudes $T_{\gamma\pi}$ will not be given here, since they are well documented [8–12].

III. THE RESULTS AT $q^2=0$ PHOTON POINT

To determine the $\gamma N\to\Delta$ form factors defined by Eq. (14), it is necessary to first fix their values at $q^2=0$ by investigating the pion photoproduction reactions. This was done in Ref. [7] by applying the formulation outlined in Sec.

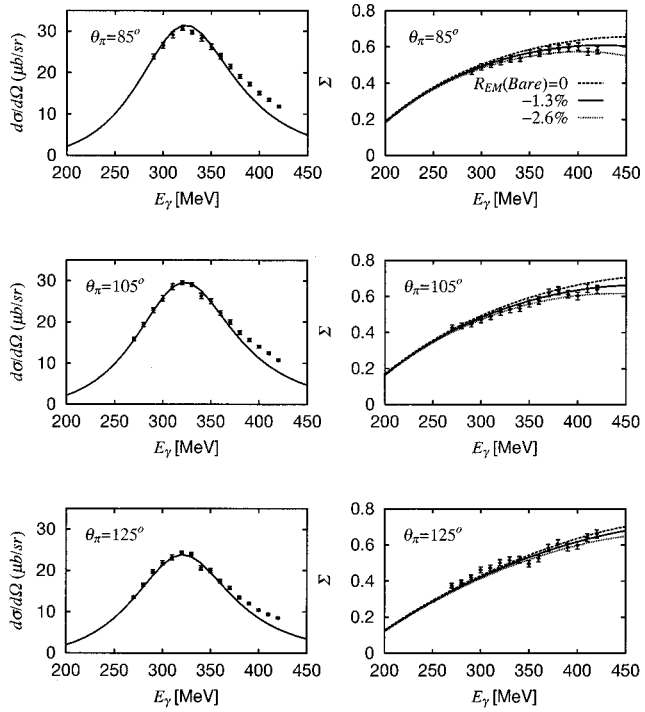

FIG. 3. The calculated differential cross section $(d\sigma/d\Omega)$ and photon asymmetry (Σ) of the $p(\gamma,\pi^0)p$ reaction are compared with the Mainz data [2]. The results from setting $R_{EM}(\text{bare}) = G_E(0)/G_M(0) = 0$, -1.3, and -2.6% with $G_M(0) = 1.85$ for the bare $\gamma N \to \Delta$ vertex are indicated in the figure. The three results for the differential cross section are not distinguishable.

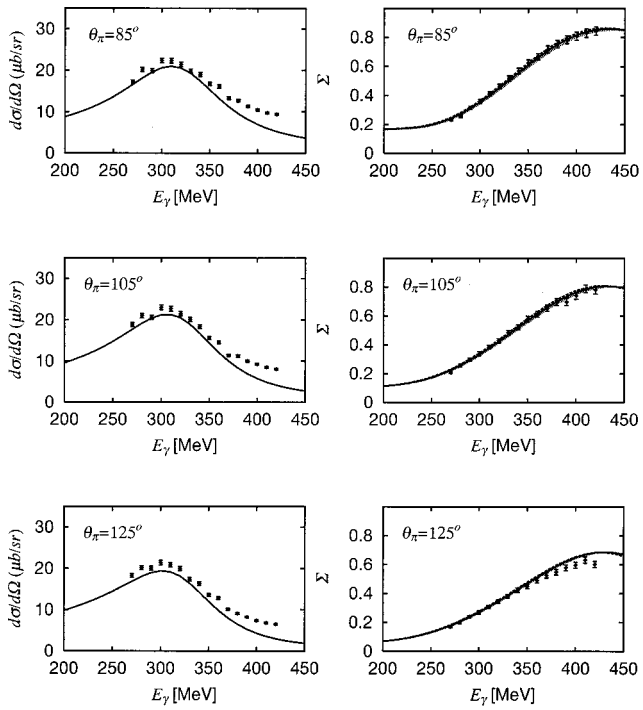

FIG. 4. Same as Fig. 3 except for the $p(\gamma,\pi^+)n$ reaction. Three results are not distinguishable here.

II. The first step was to investigate the πN scattering from threshold to the Δ excitation region. By fitting the πN phase shifts, the parameters characterizing the strong interaction vertices except the ωNN vertex in Fig. 2 were determined. The pion photoproduction data were then used to determine $G_M(0)$ and $G_E(0)$ of the $\gamma N \to \Delta$ transition [Eq. (14)] and the coupling constant $g_{\omega NN}$ of the ωNN vertex of Fig. 2.

It will be ideal if we can fix the $g_{\omega NN}$ coupling constant by using the experimental information about the nonresonant interactions. This will be possible if the ''accurate'' and ''model-independent'' empirical multipole amplitudes can be extracted from the data of the $\gamma N \to \pi N$ reactions. Unfortunately, there exist considerable disagreements between the nonresonant amplitudes from different amplitude analyses [27,47,48]. This is mainly due to the fact that the ''complete measurements'' are not available and each amplitude analysis has its own assumptions in parametrizing the full amplitudes which are more than the generally accepted amplitudes due to the Born terms and vector meson exchanges. Furthermore each analysis used different database. In our opinion, the existing empirical nonresonant amplitudes are not sufficiently accurate and model-independent for a quantitative determination of the value of $g_{\omega NN}$ within our model. Therefore we determine our only three parameters $G_M(0)$, $G_E(0)$, and $g_{\omega NN}$ by directly fitting the ''original'' experimental data. This is also the procedure we used in Ref. [7].

In Ref. [7] we considered previous pion photoproduction data [49] and the LEGS data [1] of photon asymmetry defined by

$$\Sigma = \frac{d\sigma_\perp - d\sigma_\parallel}{d\sigma_\perp + d\sigma_\parallel}, \tag{30}$$

where $d\sigma_\perp (d\sigma_\parallel)$ are the cross sections with photons linearly polarized in the direction perpendicular (parallel) to the reaction plane. To refine our model, we consider the recent Mainz data [2] here. For the photon asymmetry Σ, the data from Mainz agree very well with that from LEGS. The main improvement we have made is from using the Mainz differential cross section $(d\sigma/d\Omega)$ data which are much more precise than the data [49] used in Ref. [7].

With the πN amplitudes calculated from the model-L of Ref. [7], we find that the Mainz data can be best reproduced by setting $G_M(0) = 1.85$, $G_E(0) = 0.025$, and $g_{\omega NN} = 11.5$. These values of $G_M(0)$ and $G_E(0)$ are identical to that determined in Ref. [7]. The ωNN coupling constant is also only slightly larger than the value 10.5 determined there. Such a small change in the determined parameters is due to the fact that the previous photoproduction data [49] are close to the Mainz data except that their errors are larger.

Our results for $\gamma p \to \pi^0 p$ and $\gamma p \to \pi^+ n$ reactions are compared with the data in Figs. 3 and 4, respectively. Clearly the agreement is satisfactory in general. For the π^0 production (Fig. 3), we also show the dependence of the calculated asymmetry Σ on the $E2/M1$ ratio of the bare $\gamma N \to \Delta$ vertex. The value $R_{EM}(\text{bare}) = -1.3\%$, which corresponds to $G_M(0) = 1.85$ and $G_E(0) = 0.025$, seems to be favored by the data. On the other hand, such a dependence is much less for the π^+ production (Fig. 4) since the nonresonant interactions

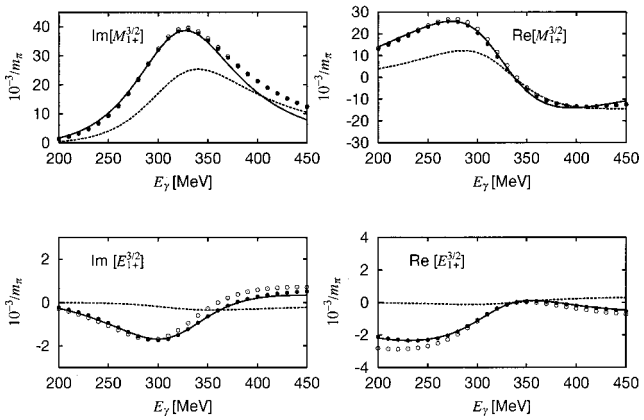

FIG. 5. The predicted $M_{1+}^{3/2}$ and $E_{1+}^{3/2}$ amplitudes for the $\gamma N \to \pi N$ reaction are compared with the results from the empirical amplitude analyses. The dotted curves are from the calculations neglecting the nonresonant interaction $v_{\gamma\pi}$. See text for more detailed description. The open circle data are from SM95 [48] and solid circle data are from Mainz98 [27].

play a more important role in this channel. There are still some discrepancies with the data. In particular, the differential cross sections at high energies $E_\gamma > 350$ MeV are underestimated. This could be due to the neglect of the coupling with higher mass nucleon resonances and two-pion production channels. For the π^+ production (Fig. 4), the cross sections at low energies are also underestimated slightly. This could be mainly due to the deficiency of our nonresonant amplitude which plays a much more important role in π^+ production than in π^0 production. Possible improvements of our model will be discussed in Sec. IV.

The results presented in the rest of this paper are from calculations with $G_M(0)=1.85$ and $G_E(0)=0.025$. In Fig. 5, we show that the predicted $M_{1+}^{3/2}$ and $E_{1+}^{3/2}$ amplitudes of the $\gamma N \to \pi N$ reactions agree very well with the data from the Mainz98 [27] and SM95 [48] analyses. By using Eqs. (28) and (29) and reading the results at resonant energy $E_\gamma = 340$ MeV displayed in Fig. 5, we find that the $E2/M1$ ratio for the dressed $\gamma N \to \Delta$ transition is $R_{EM} = -2.7\%$. The dotted curves in Fig. 5 are obtained from setting the nonresonant interaction $v_{\gamma\pi}$ to zero in the calculations. Clearly the nonresonant mechanism has a crucial role in determining the electromagnetic excitation of the Δ. At the resonance energy $E_\gamma = 340$ MeV the bare Δ amplitude is about 60% of the full amplitude for the $M1$ transition and almost a half for the $E2$ transition. As discussed in Refs. [7,32], this large difference between the bare Δ and full amplitudes is the source of the discrepancies between the quark model predictions of the $\gamma N \to \Delta$ transition and the values determined from the empirical amplitude analyses such as those listed by PDG [36]. Our predictions of the nonresonant amplitudes agree with the general features of the existing solutions of various amplitude analyses [27,47,48]. However, those empirical values are not sufficiently ''model-independent'' and ''accurate'' for learning more about the dynamical content of our model. Therefore, no comparison of our predictions with the empirical nonresonant amplitudes will be discussed here (our full amplitudes are available upon request).

TABLE I. Helicity amplitude $A_{3/2}$ and $E2/M1$ ratio R_{EM} for the $\gamma N \to \Delta$ transition at $Q^2=0$ photon point. $A_{3/2}$ is in unit of 10^{-3} GeV$^{-1/2}$ and R_{EM} in %. The references are (a) this work; (b) [21]; (c) [24]; (d) [27]; (e) [33]; (f) [34]; (g) [35].

	$A_{3/2}$		R_{EM}		Refs.
	Dressed	Bare	Dressed	Bare	
Dynamical model	-228	-153	-2.7	-1.3	(a)
	-256	-136	-2.4	0.25	(b)
K matrix	-255		-2.1		(c)
Dispersion	-252		-2.5		(d)
Quark model		-186		~ 0	(e)
		-157		~ 0	(f)
		-182		-3.5	(g)

In Table I, we list our results for the helicity amplitude $A_{3/2}$ and $E2/M1$ ratio of the $\gamma N \to \Delta$ transition and compare them with the results from other approaches. We see that the dressed $E2/M1$ values from different approaches are very close. For our model and the model of Ref. [21], the large differences between the dressed and bare values are evident, indicating the importance of the nonresonant mechanisms in determining the $\gamma N \to \Delta$ transition. The bare values are clearly close to the quark model predictions. Our dressed value of $A_{3/2}$ is lower than the empirical value. This is due to the fact that the width of the Δ is $\Gamma_\Delta = 93$ MeV within our model. This is smaller than the value $\Gamma_\Delta = 115$ MeV used in the empirical analyses. If we use $\Gamma_\Delta = 115$ MeV, we then have $A_{3/2} = -254$ for the dressed vertex, which agrees with the empirical analyses. On the other hand, the results presented in Table I are the direct consequence of our model. The smaller width is related to the discrepancies with the data of the differential cross sections in Figs. 3 and 4 and the empirical values of $\mathrm{Im}(M_{1^+}^{3/2})$ in Fig. 5 at $E_\gamma >$ about 350 MeV. The difference in the width Γ_Δ however does not affect the predicted ratios, as seen from Eqs. (28) and (29). With $G_M(0)$ and $G_E(0)$ determined, we can then investigate the pion electroproduction reactions.

IV. PION ELECTROPRODUCTION

With the matrix element $T_{\gamma\pi}$ calculated by using the formula outlined in Sec. II, it is straightforward to calculate various observables for pion electroproduction reactions. The needed formulation is well documented; see, for example, Refs. [8–12]. We therefore will only give explicit formulas which are needed for discussing our results.

We first consider the unpolarized differential cross sections of the $\gamma^* N \to \pi N$ transition, where γ^* denotes the virtual photon. In the usual convention [10], it is defined by

$$\frac{d\sigma}{d\Omega_\pi} = \frac{d\sigma_T}{d\Omega_\pi} + \epsilon \frac{d\sigma_L}{d\Omega_\pi} + \sqrt{2\epsilon(1+\epsilon)}\,\frac{d\sigma_I}{d\Omega_\pi}\cos\phi_\pi + \epsilon \frac{d\sigma_P}{d\Omega_\pi}\cos 2\phi_\pi, \tag{31}$$

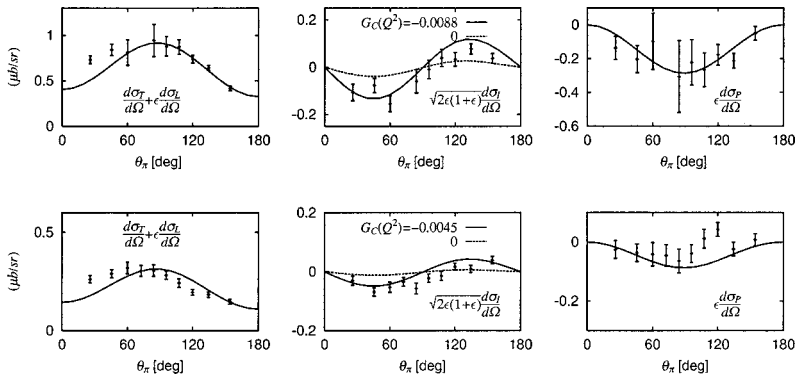

FIG. 6. Three components of the calculated $p(e,e'\pi^0)$ differential cross section [Eq. (31)] at $Q^2=2.8$ (upper row), 4.0 (lower row) $(\mathrm{GeV}/c)^2$ and $W=1235$ MeV are compared with the data which are extracted from the JLab data [3] (some of these original data are shown in Figs. 7–9).

where various differential cross sections depend on the pion scattering angle θ_π, photon momentum-square $q^2=-Q^2=\omega^2-\vec{q}^{\,2}$, and the invariant mass W of the final πN system. ϕ_π is the off-plane scattering angle between the $\pi-N$ plane and the $e-e'$ plane. The dependence of Eq. (31) on the angle θ_e between the outgoing and incoming electrons is in the parameter $\epsilon=[1+(2|\vec{q}^{\,2}|/Q^2)\tan^2\frac{1}{2}\theta_e]^{-1}$. Recalling Eq. (2.14) of Ref. [10], we note here that the transverse cross section σ_T and polarization cross section σ_P are only determined by the transverse currents J_x and J_y and the longitudinal cross section σ_L only by the longitudinal current J_z. On the other hand, the interference cross section σ_I is determined by the real part of the product $J_xJ_z^*$. In general, the contributions from the longitudinal current are much weaker than that from the transverse currents. Thus the longitudinal current can be more effectively studied by investigating the observables which are sensitive to σ_I. This has been achieved in the recent experiments at MIT-Bates and JLab by utilizing the ϕ_π dependence in Eq. (31).

To proceed, we need to define the strength of the $C2$ form factor at $q^2=0$. Here we use the well-known long wavelength limit of the multipole amplitudes to relate $E2$ and $C2$ form factors. This can be done by using Eq. (14) and the standard definitions [39] of the multipole amplitudes to obtain

$$fG_E(q^2)=\frac{\sqrt{4\pi}}{4\sqrt{2}}\langle\Delta|||T_2^{el}|||N\rangle \tag{32}$$

$$f\frac{q}{m_\Delta}G_C(q^2)=\frac{\sqrt{12\pi}}{4}\langle\Delta|||M_2^{coul}|||N\rangle, \tag{33}$$

with $f=3eqm_\Delta/(2m_N)/\sqrt{4E_N(q)m_\Delta(1-q^2/(m_N+m_\Delta)^2)}$ and the multipole operators T_2^{el},M_2^{coul} are defined in [39]. Using the long wavelength limit in Eq. (A15) of [39], we obtain a relation $G_C(q^2)=-(2m_\Delta/[m_\Delta-E_N(\vec{q})])G_E(q^2)=-(2m_\Delta/\omega)G_E(q^2)$. It follows that $G_C(0)=-[4m_\Delta^2/(m_\Delta^2-m_N^2)]G_E(0)$ simply because the resonant kinematics $m_\Delta=\omega+E_N(\vec{q})$ and $q^2=0$ lead to $\omega=(m_\Delta^2-m_N^2)/2m_\Delta$. We further note that by using the above relation, Eqs. (16) and (17) lead to $(\omega/|\vec{q}|)A_C(0)=A_E(0)$, which is consistent with the low energy limit $L_{1^+}^{3/2}\sim E_{1^+}^{3/2}$ given in Refs. [40,42,43]. [Note that A_C and A_E are related to $S_{1^+}^{3/2}$ and $E_{1^+}^{3/2}$ amplitudes, as seen in Eqs. (25)–(27), and $L_{1^+}^{3/2}=(\omega/|\vec{q}|)S_{1^+}^{3/2}$.] With $G_E(0)=+0.025$ determined in Sec. III, we thus have $G_C(0)=-0.238$.

Next we consider the JLab $p(e,e'\pi^0)$ data [3] at $Q^2=2.8$, 4 $(\mathrm{GeV}/c)^2$. Since the data are extensive enough, we are able to extract each ϕ_π-dependent term in Eq. (31). We

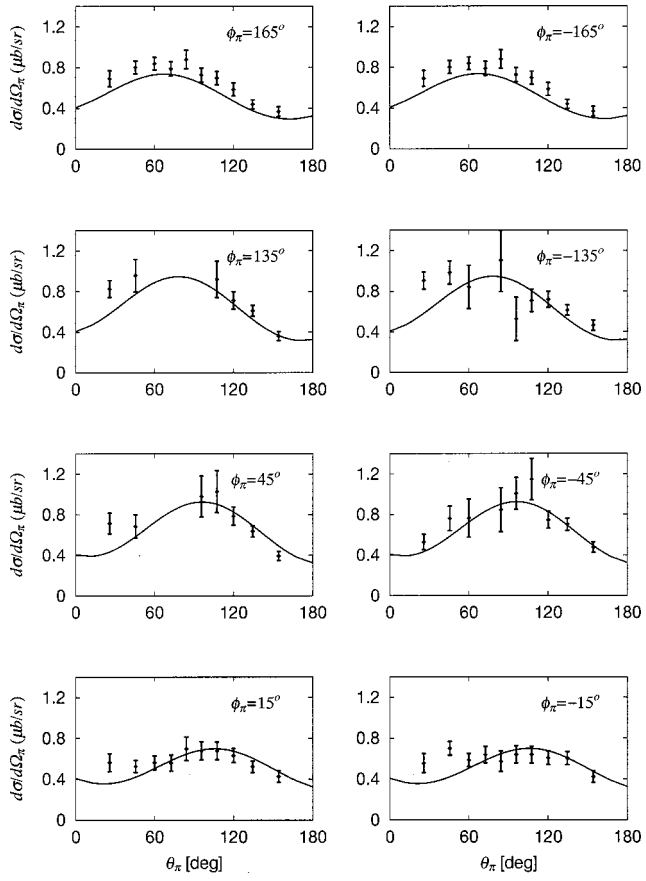

FIG. 7. The predicted $p(e,e'\pi^0)$ differential cross sections at $W=1235$ MeV and $Q^2=2.8$ $(\mathrm{GeV}/c)^2$ are compared with the JLab data [3].

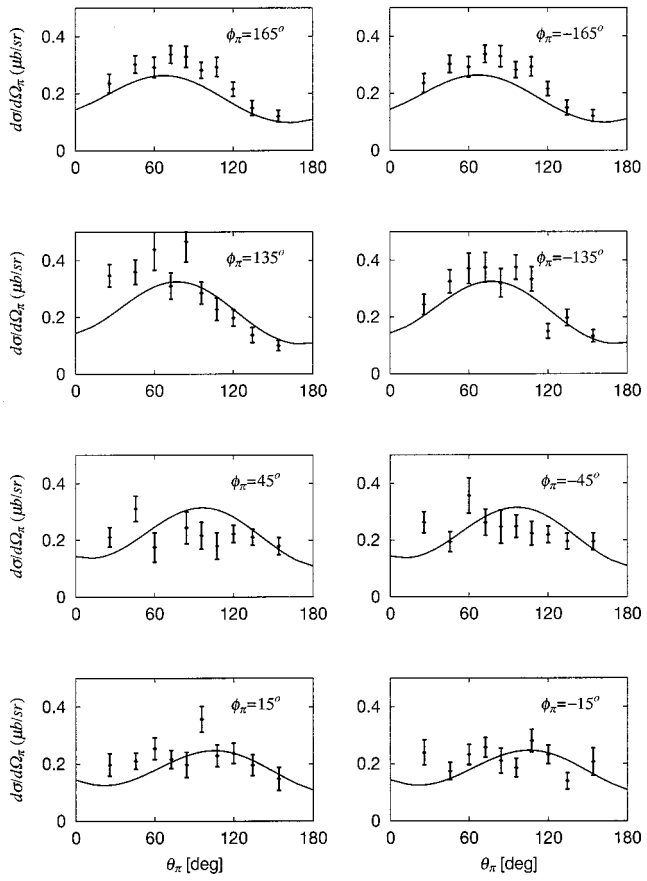

FIG. 8. Same as Fig. 7 except for $Q^2=4$ $(\mathrm{GeV}/c)^2$.

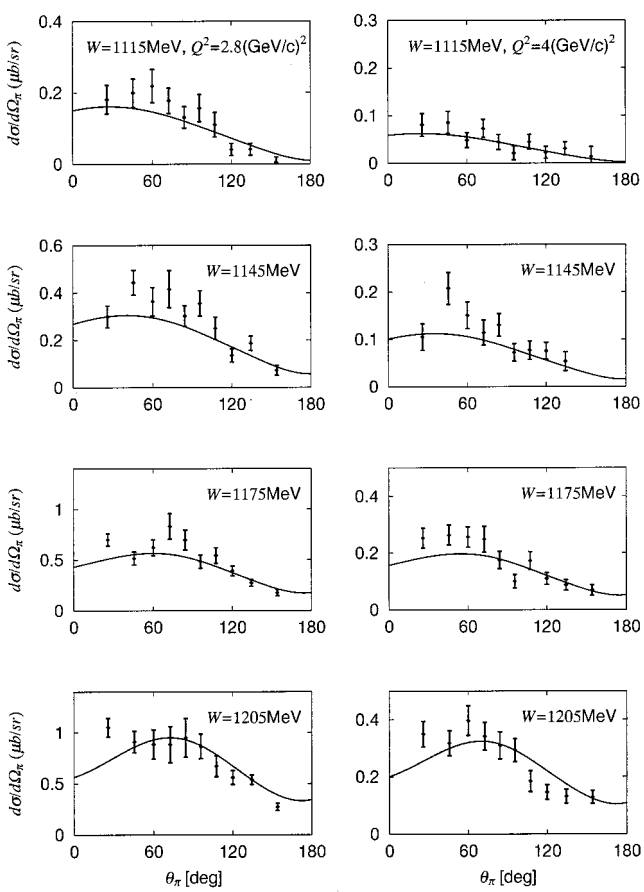

FIG. 9. The predicted $p(e,e'\pi^0)$ differential cross sections at $\phi_\pi=135°$ with $Q^2=2.8$ (left) and 4 (right) $(\mathrm{GeV}/c)^2$ are compared with the JLab data [3].

then adjust $G_M(Q^2)$, $G_E(Q^2)$, and $G_C(Q^2)$ to fit the data of these extracted components. Our best fits are the solid curves shown in Fig. 6. We also show that the interference cross section $d\sigma_I/d\Omega$ [which is determined by $\mathrm{Re}(J_x J_z^*)$] is sensitive to the charge form factor G_C of the bare $\gamma N\to\Delta$ vertex. In Figs. 7 and 8, we show the comparison with the original data at several off-plane-angle ϕ_π. Clearly the agreement is satisfactory. Similar good agreement with the data at different W are also found. Some typical results are shown in Fig. 9 for $W=1115$, 1145, 1175, and 1205 MeV.

We follow Refs. [10,21] to fit the determined form factor values at $Q^2=0$, 2.8, and 4 $(\mathrm{GeV}/c)^2$ with the following simple parametrization:

$$G_\alpha(Q^2)=G_\alpha(0)G_D(Q^2)R_\alpha(Q^2), \tag{34}$$

with $\alpha=M,E,C$ and

$$G_D(Q^2)=\left(\frac{1}{1+Q^2/0.71(\mathrm{GeV}/c)^2}\right)^2 \tag{35}$$

is the usual proton form factor. We find that our results can be fitted by choosing

$$R_\alpha(Q^2)=(1+aQ^2)\exp(-bQ^2), \tag{36}$$

with $a=0.154$ and $b=0.166$ $(\mathrm{GeV}/c)^2$ for $\alpha=M$ and C. The unpolarized cross section data are less sensitive to G_E. Nevertheless, the allowed $G_E(Q^2)$ values at $Q^2=0$, 2.8, and 4 $(\mathrm{GeV}/c)^2$ seem to also follow Eq. (36). For simplicity, we use Eq. (36) for $\alpha=M$, E and C in all of the calculations presented below. This simple parametrization is similar to that used in Ref. [21]. Equation (34) then allows us to make predictions for other values of Q^2. Note that with $a=0.154$ and $b=0.166$ $(\mathrm{GeV}/c)^2$, the Q^2 dependence due to $R_\alpha(Q^2)$ is very small compared with the dipole form factor $G_D(Q^2)$ in Eq. (35).

To further explore the Δ excitation within our model, we show in Fig. 10 the Q^2 dependence of the predicted $\gamma^*N\to\pi N$ multipole amplitudes $M_{1^+}^{3/2}$, $E_{1^+}^{3/2}$, and $S_{1^+}^{3/2}$ at $W=1232$ MeV where the πN phase shift in P_{33} channel reaches 90°. Hence, their real parts are negligibly small and are omitted in Fig. 10. These amplitudes are proportional to the dressed $\gamma N\to\Delta$ transition strengths $\bar{A}_M$, $\bar{A}_E$, and $\bar{A}_C$, as defined by Eqs. (25)–(27). We also show the results (dotted curves) from neglecting the nonresonant interaction $v_{\gamma\pi}$ in the calculations. It is interesting to note from Fig. 10 that the nonresonant interaction $v_{\gamma\pi}$ enhances strongly these amplitudes at low Q^2, but much less at high Q^2.

From the results (solid curves) shown in Fig. 10 and Eqs. (28) and (29), we obtain the Q^2 dependence of the $E2/M1$ ratio R_{EM} and $C2/M1$ ratio R_{SM} for the dressed $\gamma N\to\Delta$

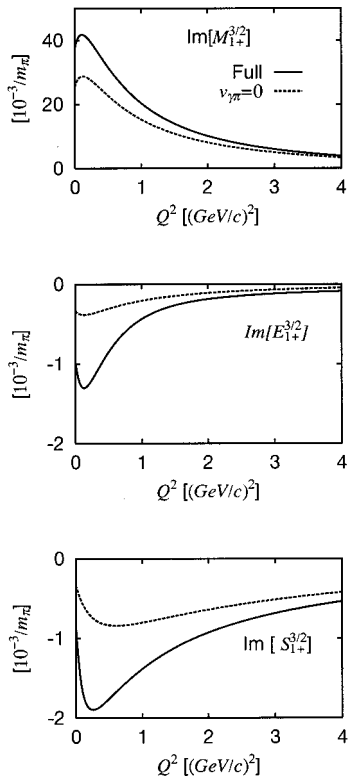

FIG. 10. Q^2 dependence of the imaginary (Im) parts of the $\gamma^* N \to \pi N$ multipole amplitudes $M_{1+}^{3/2}$, $E_{1^+}^{3/2}$, and $S_{1+}^{3/2}$ at $W=1232$ MeV. The solid curves are from our full calculations, and the dotted curves are from calculations with the nonresonant interaction $v_{\gamma\pi}$ set to zero. The real parts at $W=1232$ MeV are negligibly small and are omitted.

transition. The results are shown in Fig. 11 and Table II. We see that R_{SM} drops significantly with Q^2 and reaches $\sim 14\%$ at $Q^2=4$ (GeV/c)^2, while R_{EM} remains $\sim -3\%$ in the entire considered Q^2 region. This difference reflects an nontrivial consequence of our dynamical treatment of the nonresonant interaction, as seen in Eq. (9). It will be interesting to test our predictions in the entire Q^2 region. Clearly, the $Q^2<4$ (GeV/c)^2 region is still far away from the perturbative QCD region where R_{EM} is expected to approach unity [50].

The dressed $\gamma N \to \Delta$ vertices at the resonant energy $W=1232$ MeV, which can be calculated from using Eqs. (25)–(27), can be cast into the form of Eqs. (15)–(17). This allows us to extract the dressed $M1$ form factor $\overline{G}_M(Q^2)$ from our results and compare it with the bare

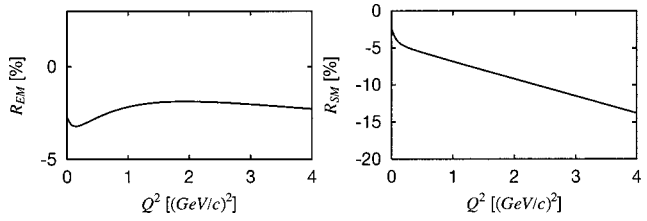

FIG. 11. The predicted Q^2 dependence of the $E2/M1$ ratio R_{EM} and $C2/M1$ ratio R_{SM} of the dressed $\gamma N \to \Delta$ form factors.

TABLE II. The Q^2 dependence of the $E2/M1$ ratio R_{EM} and $C2/M1$ ratio R_{SM} for the dressed $\gamma N \to \Delta$ transition calculated from this work.

Q^2 (GeV/c)^2	0	0.1	1	2	3	4
R_{EM} (%)	-2.7	-3.2	-2.2	-1.9	-2.0	-2.3
R_{SM} (%)	-2.3	-4.1	-6.8	-9.2	-11	-14

form factor $G_M(Q^2)$ of Eq. (14). This is shown in Fig. 12 where we measure their Q^2 dependence against the proton dipole form factor $G_D(Q^2)$ defined in Eq. (35). Here we plot $G_M^*(Q^2)=G_M(q^2)/(1+Q^2/(m_\Delta+m_N))^{1/2}$ and $\overline{G}_M^*(Q^2)=\overline{G}_M(q^2)/(1+Q^2/(m_\Delta+m_N))^{1/2}$ and scale our predictions by $\sqrt{\Gamma_\Delta^{exp}/\Gamma_\Delta^{SL}}=\sqrt{115/93}$ in order to also compare with the data from previous works [51] ($\Gamma_\Delta^{SL}=93$ MeV is the width from our model and $\Gamma_\Delta^{exp}=115$ MeV is the width used in extracting the form factor from the data).

In Fig. 12, we first observe that the Q^2 dependence of the predicted dressed form factor is in good agreement with that extracted from previous works [51]. It is also clear that both the bare and dressed $M1$ form factors drop faster than the proton form factor. The difference between the solid and dotted curves is due to the nonresonant term [see Eq. (9)] which can be interpreted as the effect due to the pion cloud around the bare quark core. This meson cloud effect accounts for about 40% of the dressed form factor at $Q^2=0$, but becomes much weaker at high Q^2. This implies that the future data at higher Q^2 will be more effective in exploring the structure of the bare quark core which can be identified with the current hadron models, as discussed in Ref. [30].

With the $\gamma N \to \Delta$ form factors given by Eqs. (34)–(36), we then can test our model by comparing our predictions with the data at other values of Q^2. We first consider the MIT-Bates data [5] at $Q^2=0.126$ (GeV/c)^2. In Fig. 13, we show the results (solid curves) for A_{LT} which is defined as [see Eq. (31)]

$$A_{LT}=\frac{\frac{d\sigma}{d\Omega_\pi}(\phi_\pi=180^\circ)-\frac{d\sigma}{d\Omega_\pi}(\phi_\pi=0^\circ)}{\frac{d\sigma}{d\Omega_\pi}(\phi_\pi=180^\circ)+\frac{d\sigma}{d\Omega_\pi}(\phi_\pi=0^\circ)}$$

$$=\frac{-\sqrt{2\epsilon(1+\epsilon)}\,\frac{d\sigma_I}{d\Omega_\pi}}{\frac{d\sigma_T}{d\Omega_\pi}+\epsilon\frac{d\sigma_L}{d\Omega_\pi}+\epsilon\frac{d\sigma_P}{d\Omega_\pi}}. \qquad (37)$$

In the same figure, we also show the results (dotted curves) from setting $G_E=G_C=0$ for the bare $\gamma N \to \Delta$ vertex [Eq. (14)]. The differences between the solid and dotted curves indicate the accuracy needed to extract these two quantities of the bare $\gamma N \to \Delta$ transition within our model.

Clearly, our predictions are close to the data at $W=1.171$ and 1.232 GeV. The result at $W=1.292$ GeV appears to disagree with the data. However our model is expected to be insufficient at this higher energy, as already seen

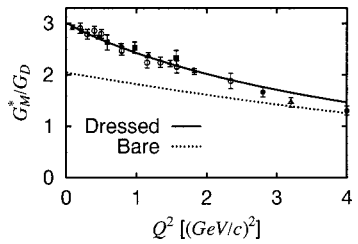

FIG. 12. The ratio between the $M1$ form factor of the $\gamma N \to \Delta$ transition and the proton dipole form factor G_D defined by Eq. (35). The solid curve is $\overline{G}_M^*(Q^2)/G_D(Q^2)$ for the dressed $M1$ form factor, and the dotted curve is $G_M^*(Q^2)/G_D(Q^2)$ for the bare $M1$ form factor. See text about the definitions of $G_M^*(Q^2)$ and $\overline{G}_M^*(Q^2)$.

in the results at $E_\gamma >$ about 350 MeV in Figs. 3 and 4 for photoproduction. It is necessary to extend our model to include additional reaction mechanisms such as the $\gamma N \to \pi\Delta \to \pi N$ transition and higher mass nucleon resonances.

In Fig. 14, we compare our results (solid curve) with the data for

$$R_{TT} = \frac{q_\gamma}{k}\left[\frac{d\sigma_T}{d\Omega} + \epsilon\frac{d\sigma_L}{d\Omega}\right]_{\theta_\pi = 180^\circ}, \tag{38}$$

where k and q_γ are the momenta for the pion and photon in the πN center of mass frame. In the same figure, we also show the results (dotted curve) obtained from neglecting the nonresonant interaction $v_{\gamma\pi}$ which renormalizes the $\gamma N \to \Delta$ vertex and generate nonresonant amplitude $t_{\pi\gamma}$, as seen in Eqs. (5), (6), and (9). The importance of the nonresonant interaction is evident. Our predictions reproduce the position

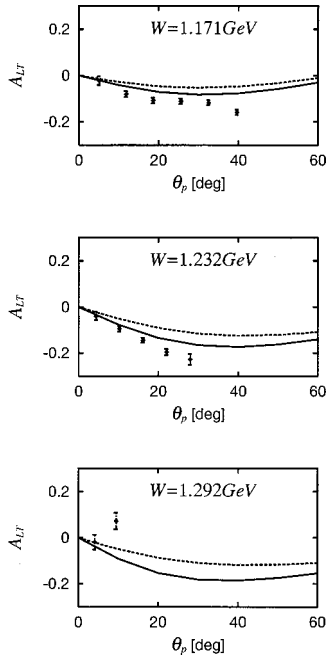

FIG. 13. The predicted asymmetry A_{LT} [Eq. (37)] of the $p(e,e'\pi^0)p$ reaction at $Q^2 = 0.126$ $(\mathrm{GeV}/c)^2$ are compared with the data from MIT-Bates [5]. The dotted curves are obtained from setting $G_M(Q^2) = G_C(Q^2) = 0$.

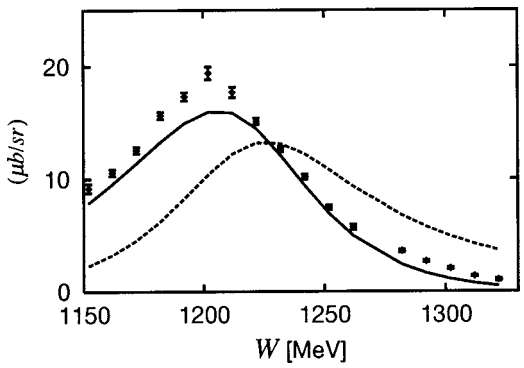

FIG. 14. The predicted R_{TT} [Eq. (38)] at $\theta_\pi = 180°$ are compared with the data from MIT-Bates [5]. The dotted curve is obtained from setting the nonresonant interaction $v_{\gamma\pi}$ to zero.

of the Δ peak which is shifted significantly by the nonresonant interaction, but underestimate the magnitude at the peak by about 15%.

In Fig. 15, we present our results for the induced proton polarization P_n for $\theta_\pi = 180°$ and the polarization vector $\vec{n}$ perpendicular to the momentum of the recoiled proton. The data at $W = 1232$ MeV is also from the measurement at MIT-Bates. Our model clearly only agrees with the data in sign, but not in magnitude. More experimental data for this observable are needed to test the energy dependence of our predictions.

The results shown in Figs. 13–15 are from the calculations using the Δ form factors given by Eqs. (34)–(36) and fitted to the data at $Q^2 = 0$, 2.8, and 4.0 $(\mathrm{GeV}/c)^2$. The chosen parametrization is rather arbitrary and there is no strong reason to believe it should give reliable predictions for the Δ form factors at the considered $Q^2 = 0.126$ $(\mathrm{GeV}/c)^2$. We therefore have explored whether the discrepancies seen in Figs. 13–15 can be removed by adjusting $G_M(Q^2)$, $G_E(Q^2)$, and $G_C(Q^2)$ for the bare $\gamma N \to \Delta$ transition. It turns out that we are not able to improve our results. It is necessary to also modify the nonresonant amplitude $t_{\gamma\pi}$. We will discuss possible improvements in the next section.

In Fig. 16, we compare our predictions with some of the Bonn data [52] at $Q^2 = 0.45$ and 0.75 GeV/c^2. Our predictions are in good agreement with these data, but these data

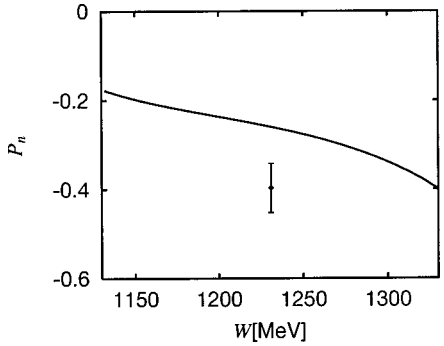

FIG. 15. The predicted induced proton polarization P_n at $\theta_\pi = 180°$ and the polarization vector $\vec{n}$ perpendicular to the recoiled proton momentum are compared with the data from MIT-Bates [5].

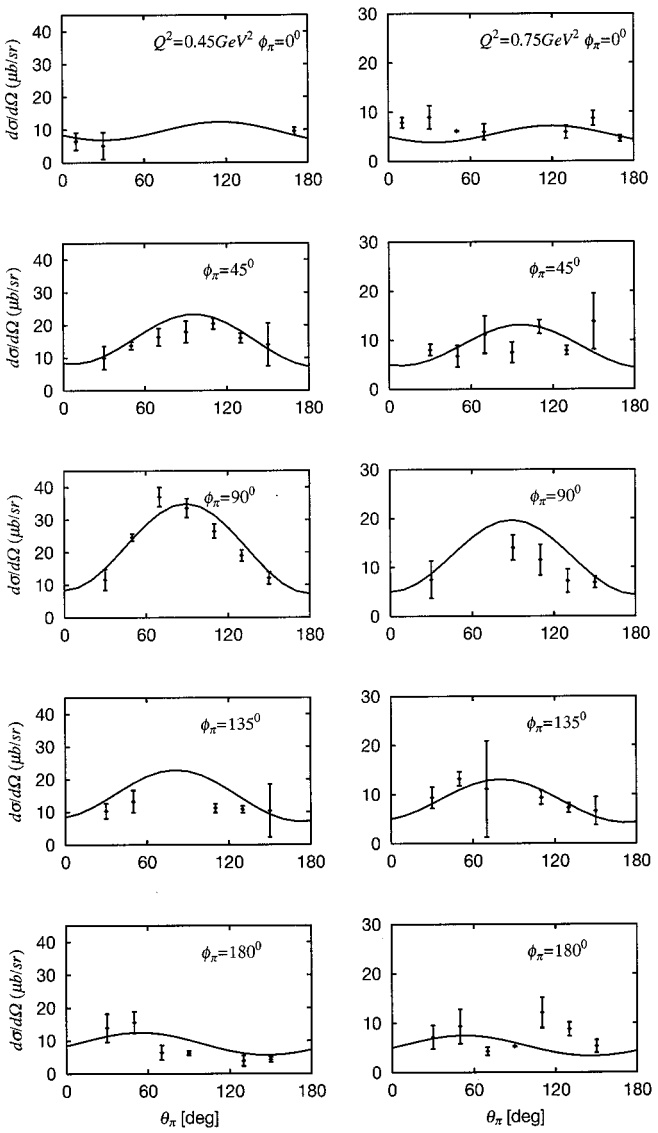

FIG. 16. The predicted differential cross sections of $p(e,e'\pi^0)$ reaction at $Q^2=0.45$ (left), 0.75 (right) $(\mathrm{GeV}/c)^2$ and $W=1232$ MeV are compared with the data [52].

have large errors. The new high-accuracy data [4] from JLab in this Q^2 region will give a more critical test of our predictions. For the forthcoming inclusive $\vec{p}(\vec{e},e')$ data from NIKHEF, we also have made the predictions at $Q^2=0.11$ $(\mathrm{GeV}/c)^2$ for two polarization observables A_{TT} and A_{TL} which are clearly defined by Eqs. (2.25b) and (2.25c) of Ref. [11]. Our predictions (solid curves) are given in Fig. 17. The dotted curves are from setting the $\gamma^*N\to\pi N$ multipole amplitudes $E_{1^+}^{3/2}$ and $S_{1^+}^{3/2}$ to zero. This gives an estimate of the required experimental accuracy in using the forthcoming data of A_{TT} and A_{TL} to extract these two amplitudes which contain information about G_E and G_C of the $\gamma N\to\Delta$ transition.

V. SUMMARY AND FUTURE DEVELOPMENTS

In this work, we have extended the dynamical model developed in Ref. [7] to investigate the pion electroproduction

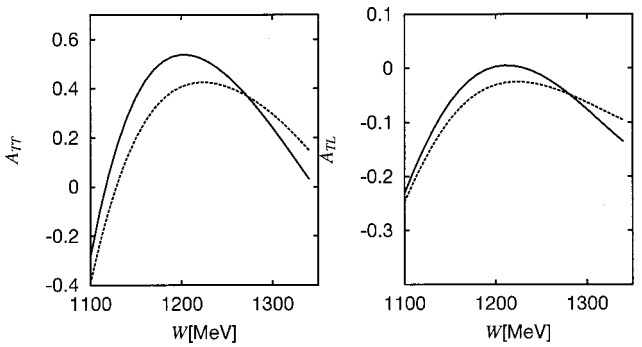

FIG. 17. The predicted A_{TT} and A_{TL}, as defined by Eqs. (2.25b) and (2.25c) of Ref. [11], for the inclusive $\vec{p}(\vec{e},e')$ reaction at $Q^2=0.11$ $(\mathrm{GeV}/c)^2$. The dotted curves are obtained when the $\gamma^*N\to\pi N$ multipole amplitudes $S_{1^+}^{3/2}$ and $E_{1^+}^{3/2}$ are not included in the calculation.

reactions. The model is first refined at the $Q^2=0$ photon point by taking into account the recent pion photoproduction data from Mainz [2]. It is found that the extracted $M1$ strength $G_M(0)=1.85$ and $E2$ strength $G_E(0)=0.025$ of the bare $\gamma N\to\Delta$ vertex are identical to that determined in Ref. [7]. By using the long wavelength limit, we then obtain $G_C(0)=-0.238$ for the charge form factor of the bare $\gamma N\to\Delta$ transition.

For the investigation of pion electroproduction, we follow the previous work to define the form factor at each photon vertex in the nonresonant interaction $v_{\gamma\pi}$ illustrated in Fig. 2. At each value of Q^2, the $\gamma N\to\Delta$ transition strengths $G_M(Q^2)$, $G_E(Q^2)$, and $G_C(Q^2)$ are the only free parameters in our calculations. We find that the recent $p(e,e'\pi^0)$ data at $Q^2=2.8$ and 4 $(\mathrm{GeV}/c)^2$ from JLab [3], and at $Q^2=0.126$ $(\mathrm{GeV}/c)^2$ from MIT-Bates [5] can be described to a very large extent if the bare $\gamma N\to\Delta$ form factors defined by Eqs. (34)–(36) are used in the calculations. It is found that the remaining discrepancies cannot be resolved by only adjusting these Δ form factors.

We focus on the investigation of the Q^2 dependence of the Δ excitation mechanism. It is found that the nonresonant interactions can dress the $\gamma N\to\Delta$ vertex to enhance strongly its strength at low Q^2, but much less at high Q^2 (Fig. 10). The determined $C2/M1$ ratio (R_{SM}) drops significantly with Q^2 and reaches $\sim 14\%$ at $Q^2=4$ $(\mathrm{GeV}/c)^2$, while the $E2/M1$ ratio (R_{EM}) remains at $\sim -3\%$ of the value at the $Q^2=0$ photon point (Fig. 11 and Table II). The determined $M1$ form factor drops faster than the usual dipole form factor of the proton (Fig. 12). This is in agreement with the previous findings [3,21].

To end, we turn to discussing possible future developments within our formulation. The model we developed in Ref. [7] and applied in this work is defined by the effective Hamiltonian (3). It is derived from using a unitary transformation method up to second order in the vertex interaction H_I [Eq. (2)]. We further assume that the πN and γN reactions can be described within a subspace $\Delta\oplus\pi N\oplus\gamma N$. From the point of view of the general Hamiltonians (1) and (2), which can be identified [30] with a hadron model, our model is clearly just a starting model. For this reason, no attempt

is made here to adjust the parameters of the nonresonant interaction $v_{\gamma\pi}$ to perform a χ^2-fit to the electroproduction data. To resolve the remaining discrepancies between our predictions and the data, it is necessary to improve our model in several directions.

To improve our results in the higher energy region (Figs. 3, 4, and 13), we need to include the coupling with other reaction channels. An obvious step is to extend the effective Hamiltonian (3) to include the transitions to ηN, $\pi\Delta$, and ρN states and to include some higher mass N^* states. The resulting scattering equations will be more complex than what are given in Ref. [7] and outlined in Eqs. (5)–(11). In particular, it will have the $\pi\pi N$ cut structure due to the $\Delta \rightarrow \pi N$ decay in the $\pi\Delta$ channel and the $\rho\rightarrow\pi\pi$ decay in the ρN channel. This $\pi\pi N$ cut must be treated exactly in any attempt to explore the structure of N^* resonances. This was well recognized in the early investigations [53] and must be pursued in a dynamical approach.

The second necessary improvement is to use more realistic form factors in defining the photon vertices of nonresonant interaction $v_{\gamma\pi}$. The prescription (12) must be relaxed. In particular we should use a form factor $F_{\gamma\pi\pi}(Q^2)$ predicted from a calculation which accounts for the off-mass-shell properties of the exchange pion in Fig. 2. Similarly, the vector meson form factor $g_{V\pi\gamma}$ [Eq. (13)] must also be improved since the exchanged vector meson is also off its mass shell. Improvement in this direction could be possible in the near future, since the calculations for such off-mass-shell form factors can now be performed within some QCD models of light mesons [54].

ACKNOWLEDGMENTS

This work was supported by U.S. DOE Nuclear Physics Division, Contract No. W-31-109-ENG and by Japan Society for the Promotion of Science, Grant-in-Aid for Scientific Research (C) 12640273.

[1] G. Blanpied *et al.*, Phys. Rev. Lett. **79**, 4337 (1997).
[2] R. Beck *et al.*, Phys. Rev. C **61**, 035204 (2000).
[3] V. V. Frolov *et al.*, Phys. Rev. Lett. **82**, 45 (1999).
[4] V. Burkert, in Proceedings of the 16th International Conference on Few-Body Problems in Physics, 1999, Taipei, Taiwan (unpublished).
[5] The data shown in this paper are from C. E. Vellidis *et al.*, in *Proceedings of the Second Workshop on Electronuclear Physics and the BLAST Detector*, edited by R. Alarcon and R. Milner (World Scientific, Singapore, 1999), p. 105; C. Mertz *et al.*, Phys. Rev. Lett. (to be published).
[6] L. D. van Buuren, in Proceedings of the 16th International Conference on Few-Body Problems in Physics [4].
[7] T. Sato and T.-S. H. Lee, Phys. Rev. C **54**, 2660 (1996).
[8] A. Donnachie, in *High Energy Physics*, edited by E. Burhop (Academic, New York, 1972), Vol. 5, p. 1.
[9] A. S. Raskin and T. W. Donnelly, Ann. Phys. (N.Y.) **191**, 78 (1989).
[10] S. Nozawa and T.-S. H. Lee, Nucl. Phys. **A513**, 511 (1990).
[11] S. Nozawa and T.-S. H. Lee, Nucl. Phys. **A513**, 543 (1990).
[12] D. Drechsel and L. Tiator, J. Phys. G **18**, 449 (1992).
[13] H. Tanabe and K. Ohta, Phys. Rev. C **31**, 1876 (1985).
[14] S. N. Yang, J. Phys. G **11**, L205 (1985).
[15] S. Nozawa, B. Blankleider, and T.-S. H. Lee, Nucl. Phys. **A513**, 459 (1990).
[16] B. Pearce and T.-S. H. Lee, Nucl. Phys. **A528**, 655 (1991).
[17] C. van Antwerpen and I. R. Afnan, Phys. Rev. C **52**, 554 (1995).
[18] Y. Surya and F. Gross, Phys. Rev. C **53**, 2422 (1996).
[19] H. Haberzettl, Phys. Rev. C **56**, 2041 (1997).
[20] K. Nakayama, Ch. Schutz, S. Krewald, J. Speth, and W. Pfeil, in *Proceedings of the Fourth CEBAF/INT Workshop on N* Physics*, edited by T.-S. H. Lee and W. Roberts (World Scientific, Singapore, 1997), p. 156.
[21] S. S. Kamalov and S. N. Yang, Phys. Rev. Lett. **83**, 4494 (1999).
[22] R. M. Davidson and N. C. Mukhopadyay, Phys. Rev. D **42**, 20 (1990); R. M. Davidson, N. C. Mukhopadyay, and R. S. Wittman, *ibid.* **43**, 71 (1990).
[23] A. Gil, J. Nieves, and E. Oset, Nucl. Phys. **A627**, 543 (1997).
[24] R. M. Davidson *et al.*, Phys. Rev. C **59**, 1059 (1999).
[25] D. Drechsel, O. Hanstein, S. S. Kamalov, and L. Tiator, Nucl. Phys. **A465**, 145 (1999).
[26] F. A. Berends, A. Donnachie, and D. L. Weaver, Nucl. Phys. **B4**, 1 (1967); **B4**, 54 (1967); **B4**, 103 (1967).
[27] O. Hanstein, D. Drechsel, and L. Tiator, Nucl. Phys. **A632**, 561 (1998).
[28] I. G. Aznauryan, Phys. Rev. D **57**, 2727 (1998).
[29] H. Feshbach, *Theoretical Nuclear Physics: Nuclear Reactions* (Wiley, New York, 1992).
[30] T. Yoshimoto, T. Sato, A. Arima, and T.-S. H. Lee, Phys. Rev. C **61**, 065203 (2000).
[31] M. Kobayashi, T. Sato, and H. Ohtsubo, Prog. Theor. Phys. **98**, 927 (1997).
[32] T.-S. H. Lee, in *Proceedings of the Fourth CEBAF/INT Workshop on N* Physics*, edited by T.-S. H. Lee and W. Roberts [20], p. 19.
[33] S. Capstick, Phys. Rev. D **46**, 1965 (1992); **46**, 2864 (1992).
[34] R. Bijker, F. Iachello, and A. Leviatan, Ann. Phys. (N.Y.) **236**, 69 (1994); Phys. Rev. C **54**, 1935 (1996).
[35] A. Buchmann, E. Hernandez, and A. Faessler, Phys. Rev. C **55**, 448 (1997).
[36] Particle Data Group, D. E. Groom *et al.*, Eur. Phys. J. C **15**, 1 (2000).
[37] H. F. Jones and M. D. Scadron, Ann. Phys. (N.Y.) **81**, 1 (1973).
[38] A. R. Edmonds, *Angular Momentum in Quantum Mechanics* (Princeton University Press, Princeton, NJ, 1957).
[39] T. deForest and J. D. Walecka, Adv. Phys. **15**, 1 (1966).
[40] E. Amaldi, S. Fubini, and G. Furlan, in Springer Tracts in Modern Physics, Vol. 83, edited by G. Höhler (Springer, Berlin, 1979), p. 1.

[41] In deriving Eqs. (15)–(17), we make use of the following relations: At the Δ peak we have $\omega+E_N(\vec{q})=m_\Delta$ and hence $E_N(\vec{q})+m_N=[(m_N+m_\Delta)^2-q^2]/2m_\Delta$. It follows that $\sqrt{[E_N(\vec{q})+m_N]/2E_N(\vec{q})}[3(m_\Delta+m_N)/(4m_N(E_N(\vec{q})+m_N)]=[1/\sqrt{2E_N(\vec{q})2m_\Delta}](3m_\Delta/2m_N)(1/[1-q^2/(m_\Delta+m_N)^2]^{1/2})$.

[42] S. Capstick and G. Karl, Phys. Rev. D **41**, 2767 (1990).

[43] See Eq. (C13) of Ref. [40] and Fig. 2 and the second paragraph of Sec. II of Ref. [42].

[44] F. Gross and D. O. Riska, Phys. Rev. C **36**, 1928 (1987).

[45] K. Ohta, Phys. Rev. C **40**, 1335 (1989).

[46] H. Haberzettl, C. Bennhold, T. Mart, and T. Feuster, Phys. Rev. C **58**, 40 (1998).

[47] A. Sandorfi (private communication).

[48] R. A. Arndt, I. I. Strakovsky, and R. L. Workman, Phys. Rev. C **53**, 430 (1996).

[49] H. Genzel *et al.*, Z. Phys. **268**, 43 (1974); D. Menze, W. Pfeil, and R. Wilcke, ZAED Compilation of Pion Photoproduction Data, University of Bonn, 1977.

[50] C. E. Carlson, Phys. Rev. D **34**, 2704 (1986).

[51] W. Bartel *et al.*, Phys. Lett. **28B**, 148 (1968); J. C. Alder *et al.*, Nucl. Phys. **B46**, 573 (1972); S. Sterin *et al.*, Phys. Rev. D **12**, 1884 (1975); V. D. Burkert and L. Elouadrhiri, Phys. Rev. Lett. **75**, 3614 (1995); V. V. Frolov *et al.*, *ibid.* **82**, 45 (1999).

[52] R. Siddle *et al.*, Nucl. Phys. **B35**, 93 (1971); J. C. Alder *et al.*, *ibid.* **B46**, 573 (1972).

[53] See review by R. Aaron, in *Modern Three-Hadron Physics*, edited by A. W. Thomas (Springer-Verlag, Berlin, Heidelberg, New York, 1977).

[54] P. Maris and P. C. Tandy, Phys. Rev. C **61**, 045202 (2000); (priviate communication).